Supporting Information

High-performance zinc-air batteries enabled by hybridizing atomically dispersed FeN_2 with Co_3O_4 nanoparticles

Fukang Gui,[a‡] Qiu Jin,[b‡] Dongdong Xiao,[c] Zehua Jin,[d] Yingchuan Zhang,[a] Yingjian Cao,[a] Ming Yang,[d] Qinggang Tan,[e] Cunman Zhang,[a] Samira Siahrostami, [b] and Qiangfeng Xiao[a]**

[a]School of Automotive Studies & Clean Energy Automotive Engineering Center, Tongji University (Jiading Campus), 4800 Cao'an Road, Shanghai 201804, China

[b]Department of Chemistry, University of Calgary, 2500 University Drive NW, Calgary, Alberta, Canada, T2N 1N4

[c]Institute of Physics, Chinese Academy of Sciences, 8 Nansan Street, Zhongguancun, Haidian District, Beijing, 100190, China

[d] Department of Chemical & Biomolecular Engineering, College of Engineering, Computing and Applied Sciences, Clemson University, 206 S. Palmetto Blvd, Clemson, SC 29634, USA

[e] School of Materials Science & Engineering, Tongji University (Jiading Campus), 4800 Cao'an Road, Shanghai, 201804, China

*Corresponding Authors. E-mail: xiaoqf@tongji.edu.cn (Q.X.); samira.siahrostami@ucalgary.ca (S.S.).

‡These authors contributed equally to this work

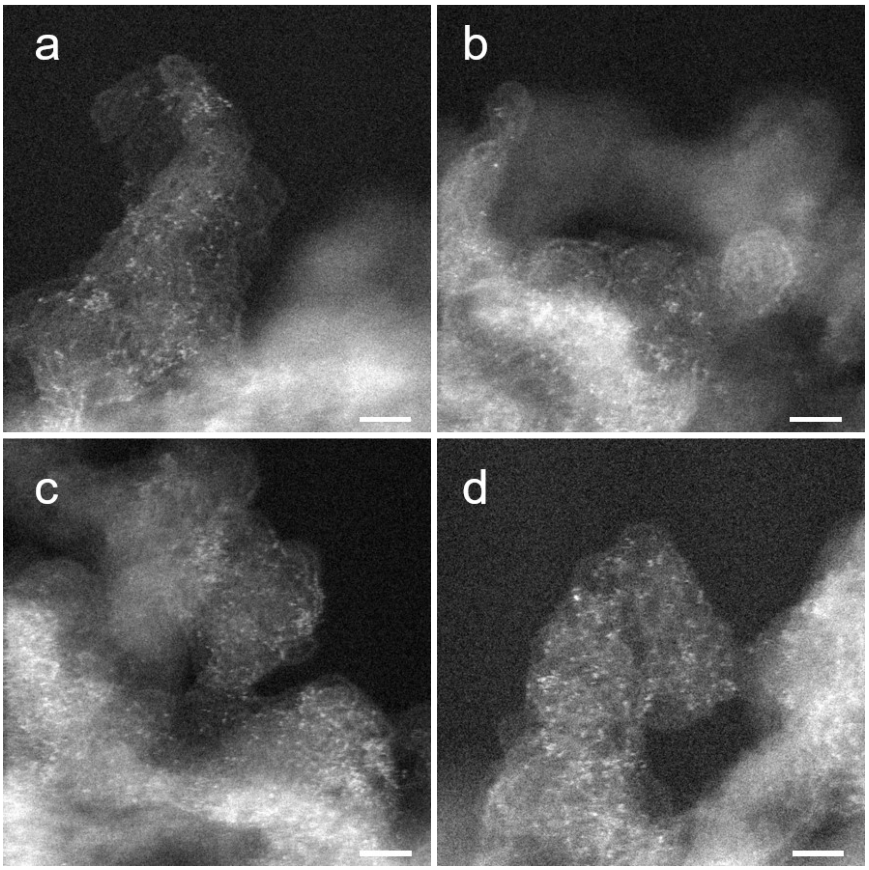

Fig. S1 (a-d) Aberration-corrected HAADF-STEM images of Fe-HPNC. Scale bar: 2 nm.

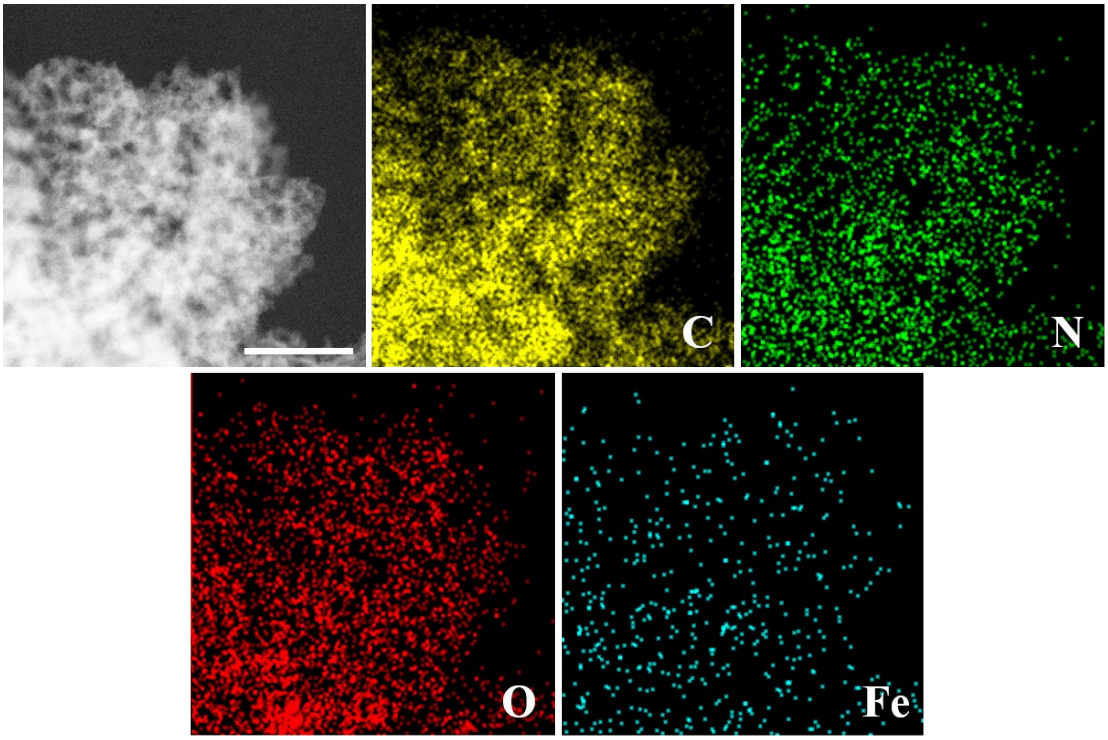

Fig. S2 STEM image and corresponding elemental mapping images of Fe-HPNC. Scale bar, 50 nm.

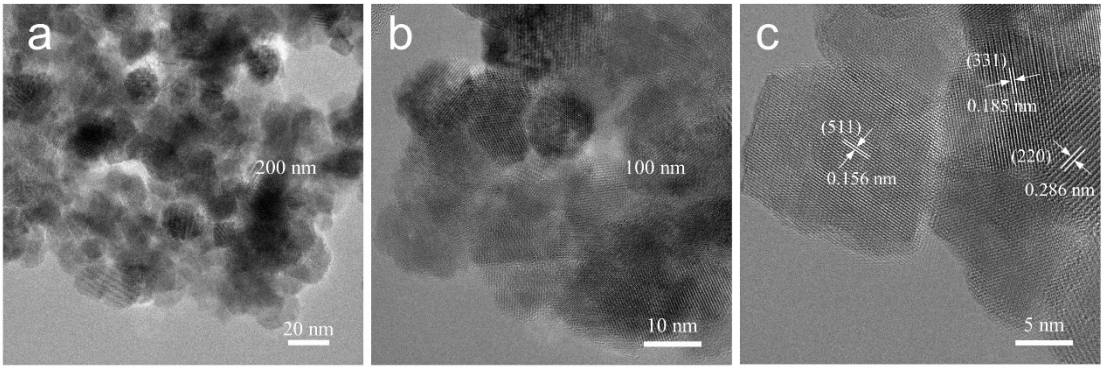

Fig. S3 (a-c) TEM and HR-TEM images of pure as-prepared Co_3O_4 nanoparticles.

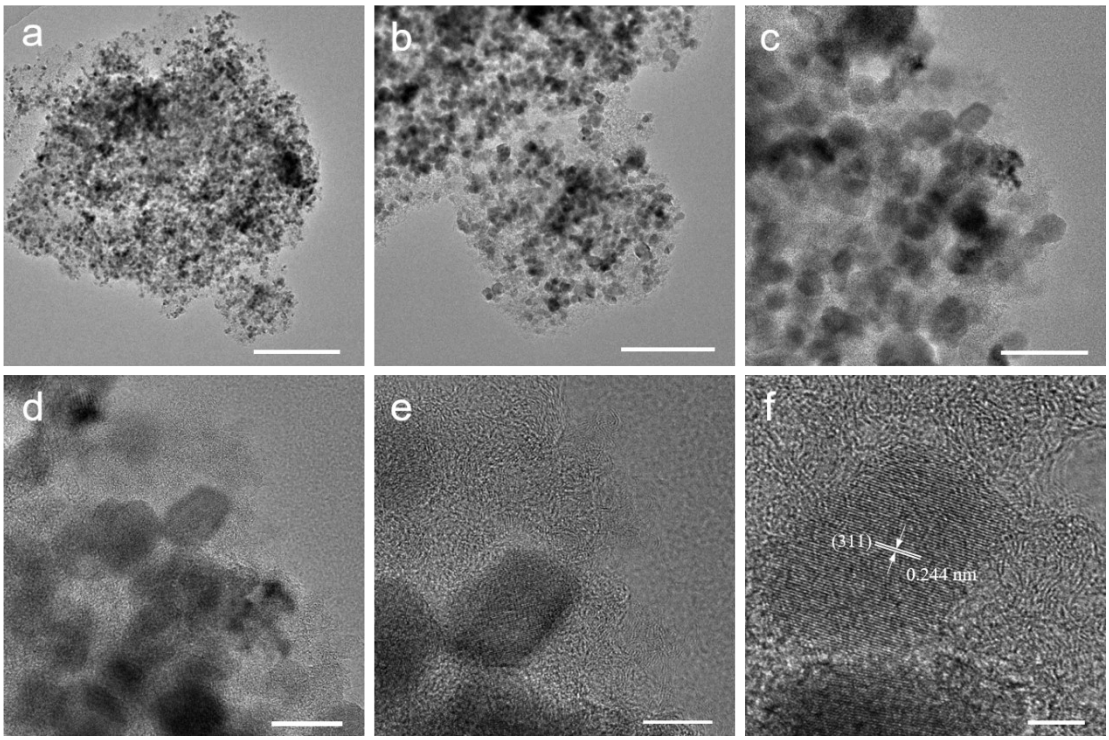

Fig. S4 (a-f) TEM and HR-TEM images of Fe-HPNC/Co_3O_4. Scale bar: (a) 500 nm, (b) 200 nm, (c) 50 nm, (d) 20 nm, (e) 10 nm, (f) 5 nm.

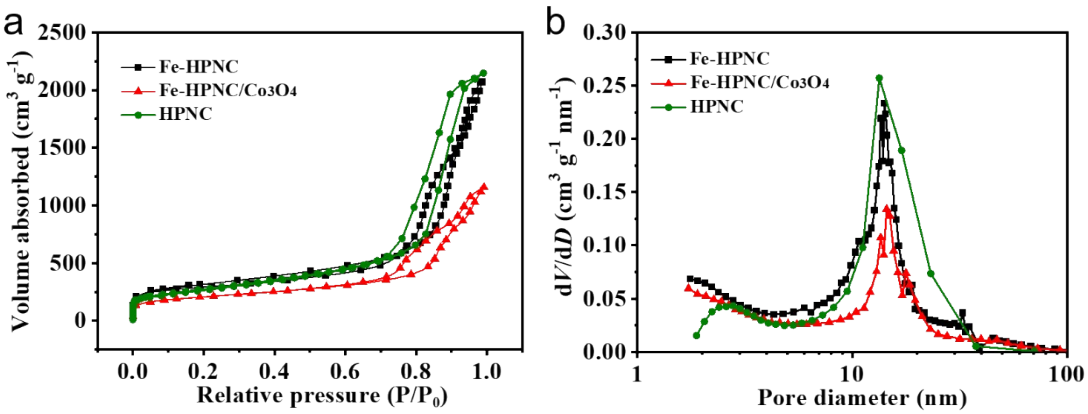

Fig. S5 (a) Nitrogen absorption-desorption isotherms and **(b)** corresponding pore size distribution curves of Fe-HPNC, Fe-HPNC/Co_3O_4 and HPNC.

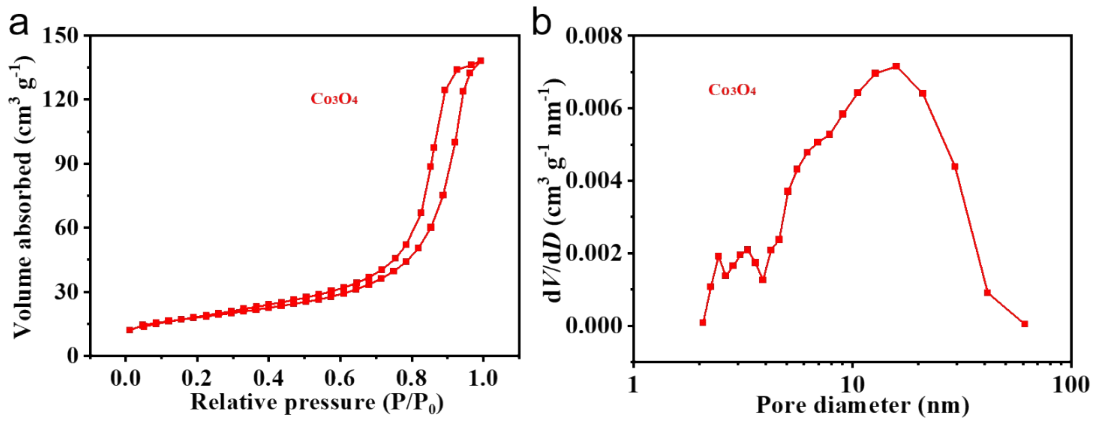

Fig. S6 (a) Nitrogen absorption-desorption isotherms and **(b)** corresponding pore size distribution curves of Co_3O_4 nanoparticles.

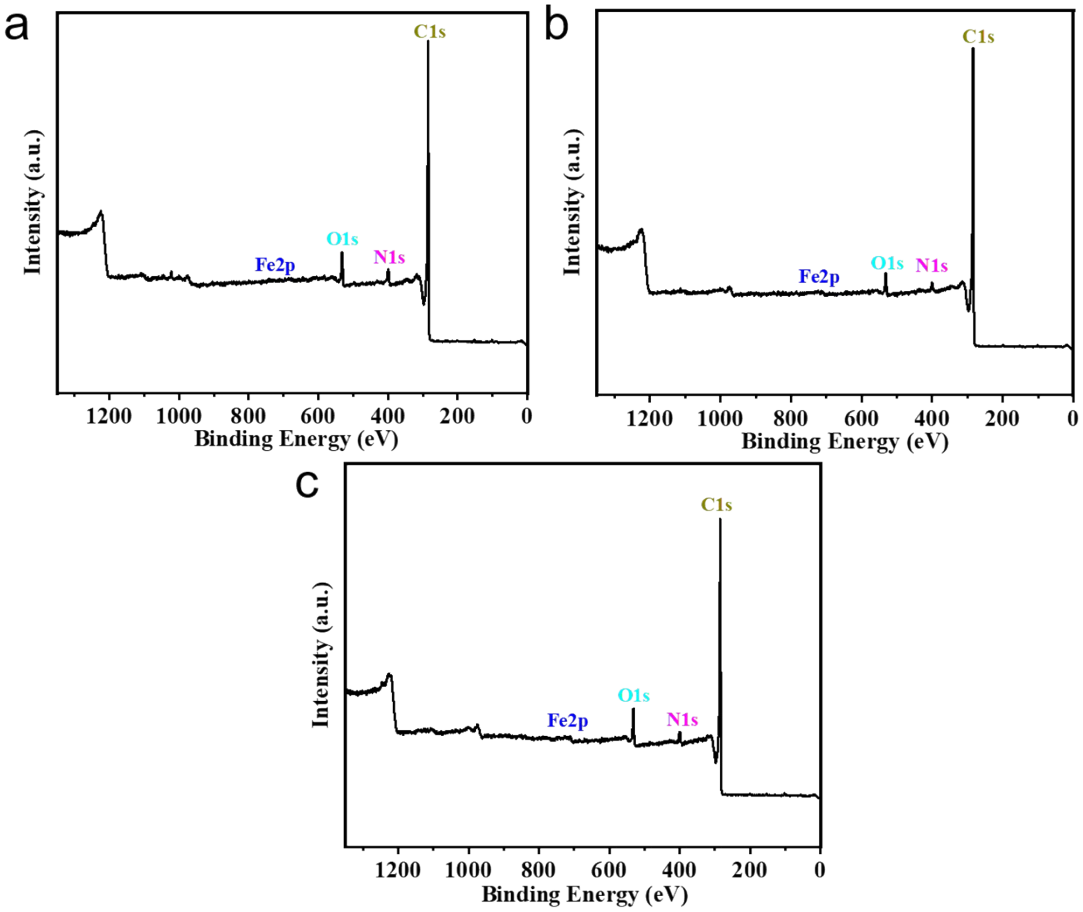

Fig. S7 XPS survey spectra of **(a)** Fe-HPNC-700, **(b)** Fe-HPNC-800 and **(c)** Fe-HPNC-900.

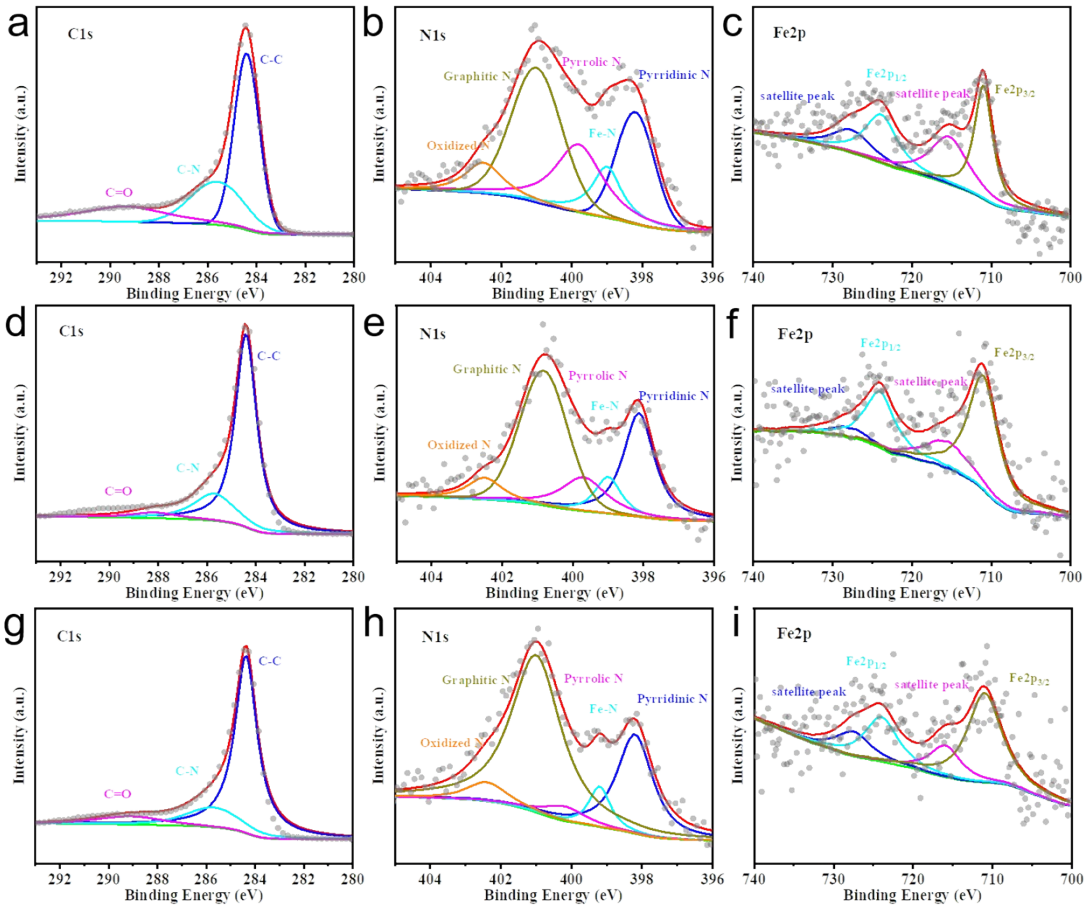

Fig. S8 High-resolution C1s, N1s and Fe 2p spectra of **(a,b,c)** Fe-HPNC-700, **(d,e,f)** Fe-HPNC-800 and **(g,h,i)** Fe-HPNC-900.

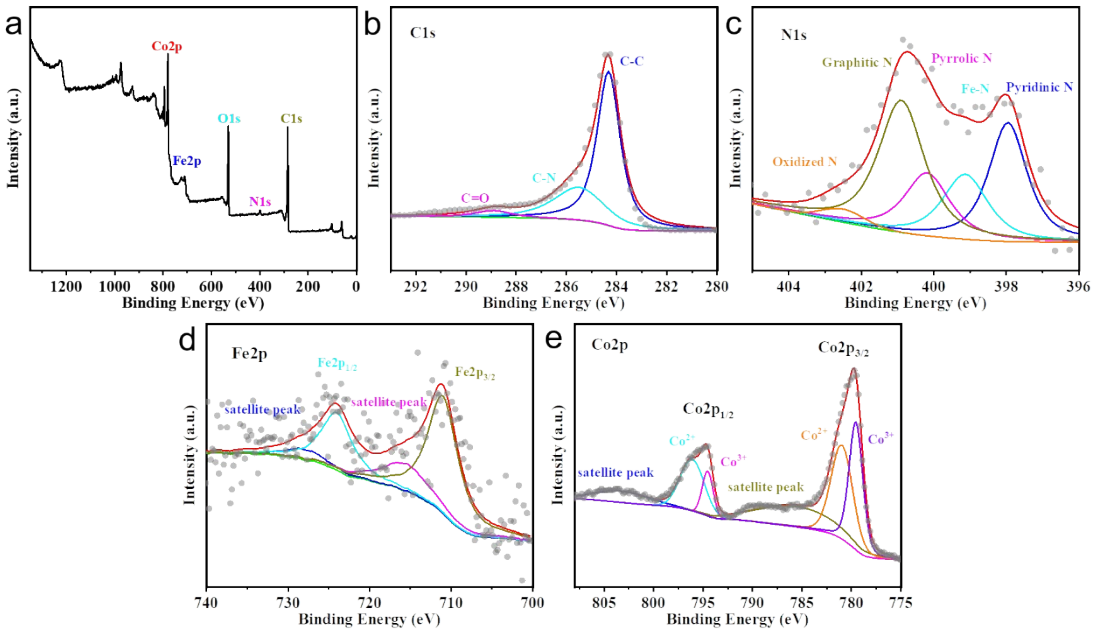

Fig. S9 (a) XPS survey spectra and high-resolution **(b)** C 1s, **(c)** N 1s, **(d)** Fe 2p and **(e)** Co 2p spectra of Fe-HPNC/Co_3O_4.

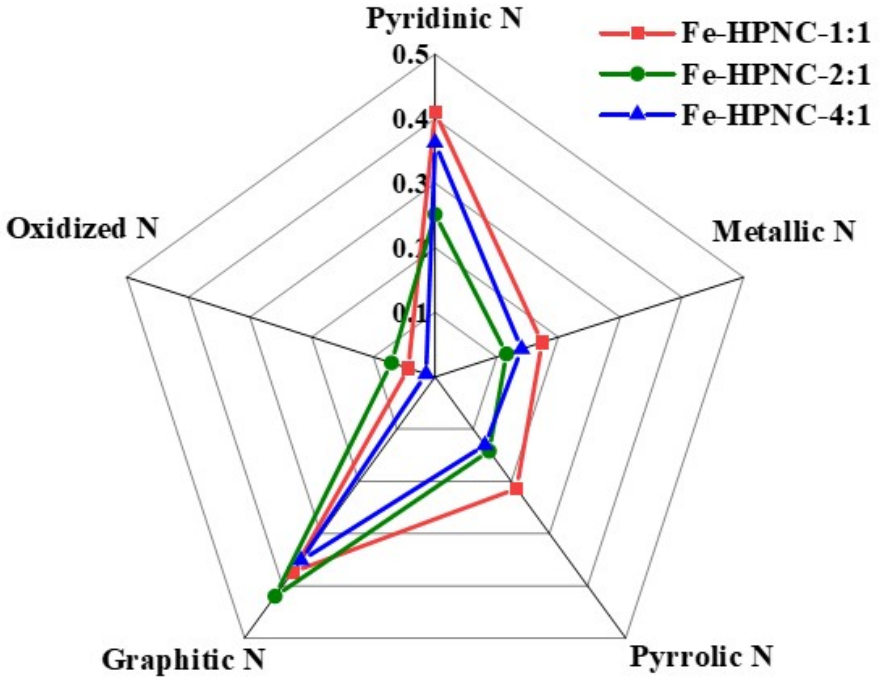

Fig. S10 Configurations of nitrogen dopants of Fe-HPNC-1:1, Fe-HPNC-2:1 and Fe-HPNC-4:1.

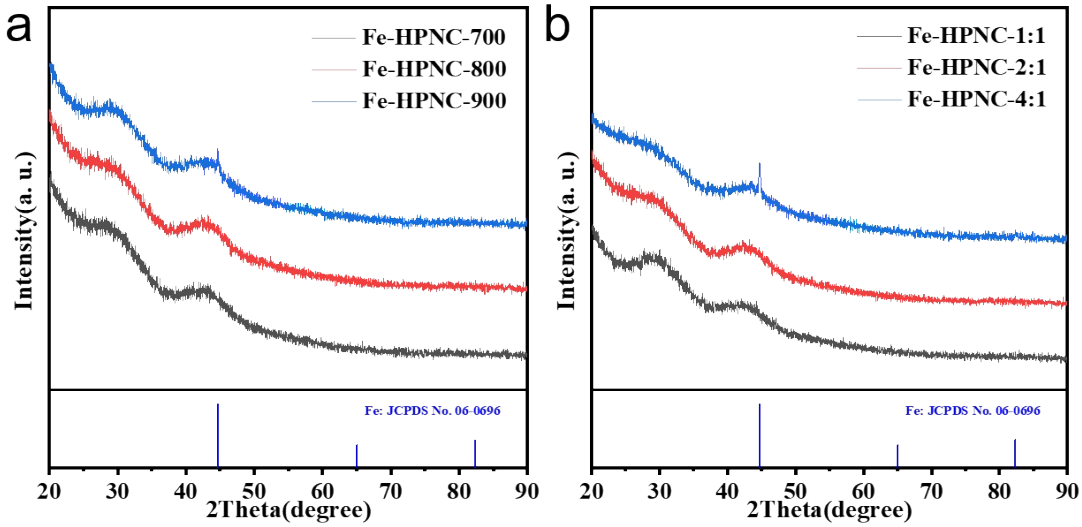

Fig. S11 XRD patterns of **(a)** Fe-HPNC-700, Fe-HPNC-800, Fe-HPNC-900 and **(b)** Fe-HPNC-1:1, Fe-HPNC-2:1 and Fe-HPNC-4:1.

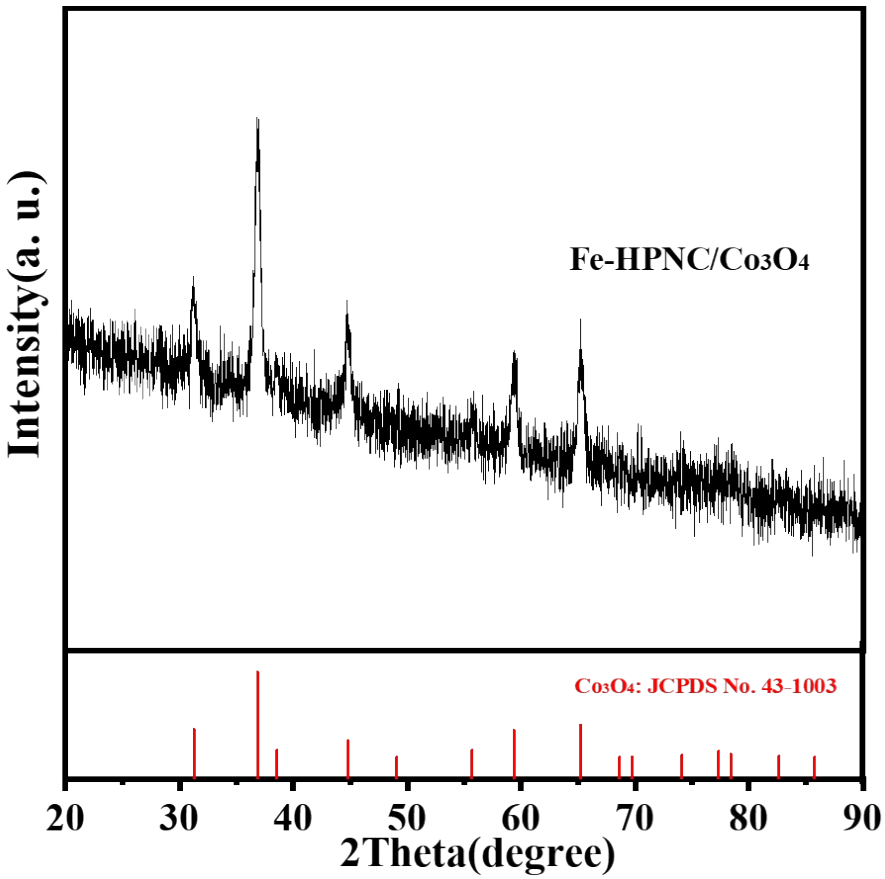

Fig. S12 XRD pattern of Fe-HPNC/Co_3O_4.

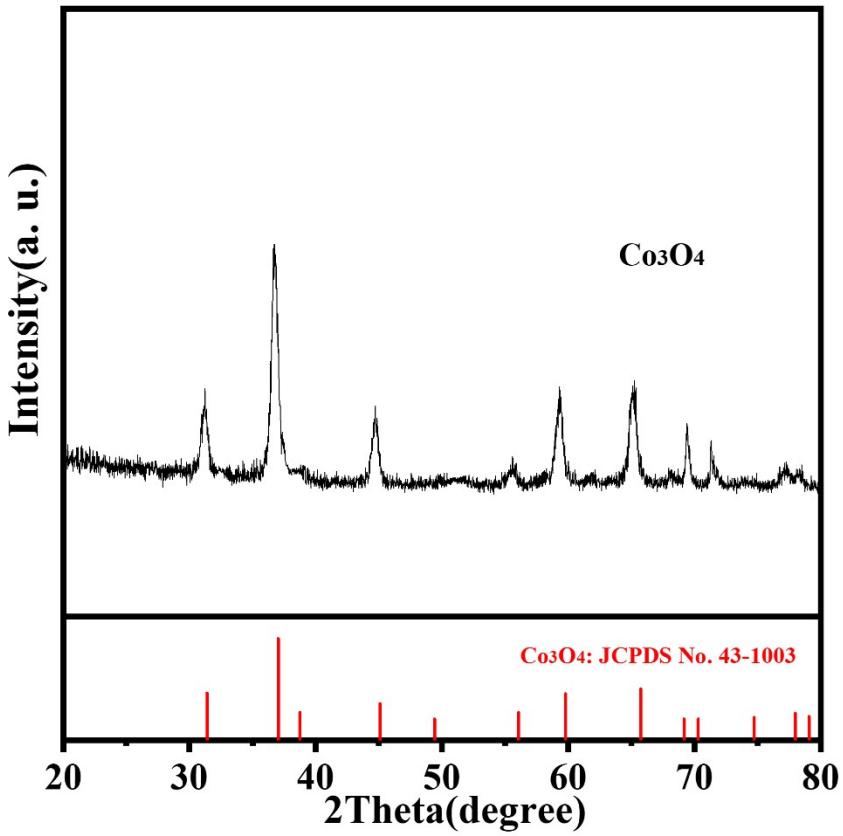

Fig. S13 XRD pattern of pure as-prepared Co_3O_4 nanoparticles.

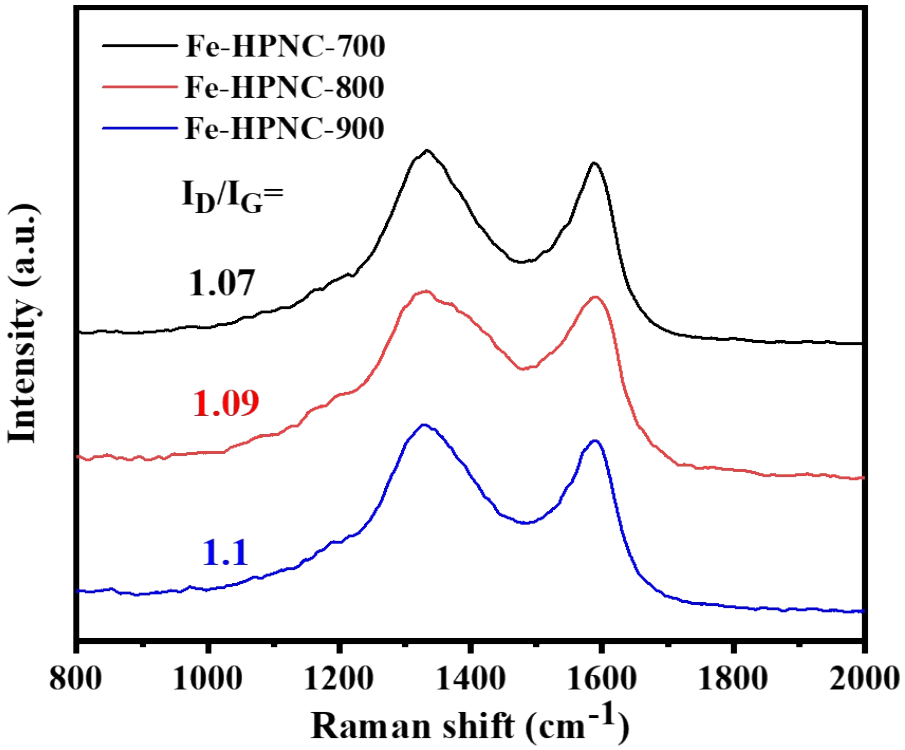

Fig. S14 Raman spectra of Fe-HPNC-700, Fe-HPNC-800 and Fe-HPNC-900.

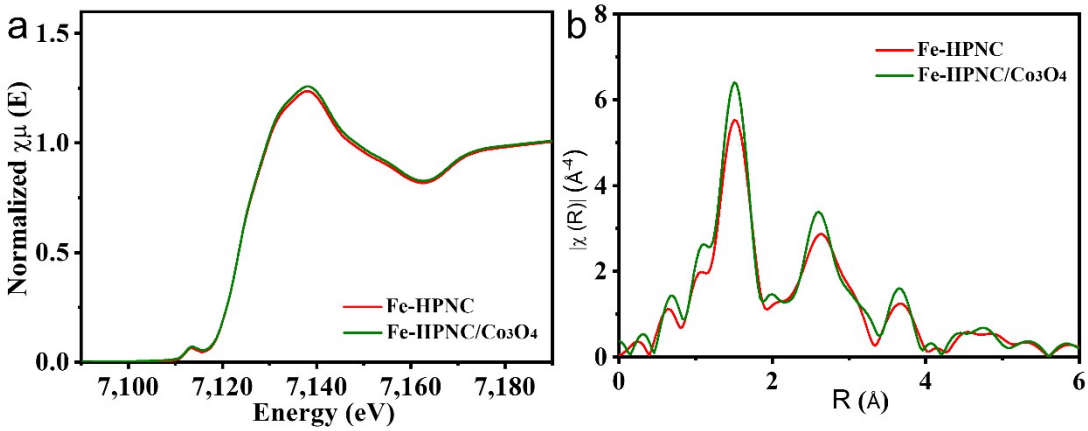

Fig. S15 Fe k-edge **(a)** XANES spectra and **(b)** Fourier-transfer EXAFS spectra of Fe-HPNC and Fe-HPNC/Co_3O_4.

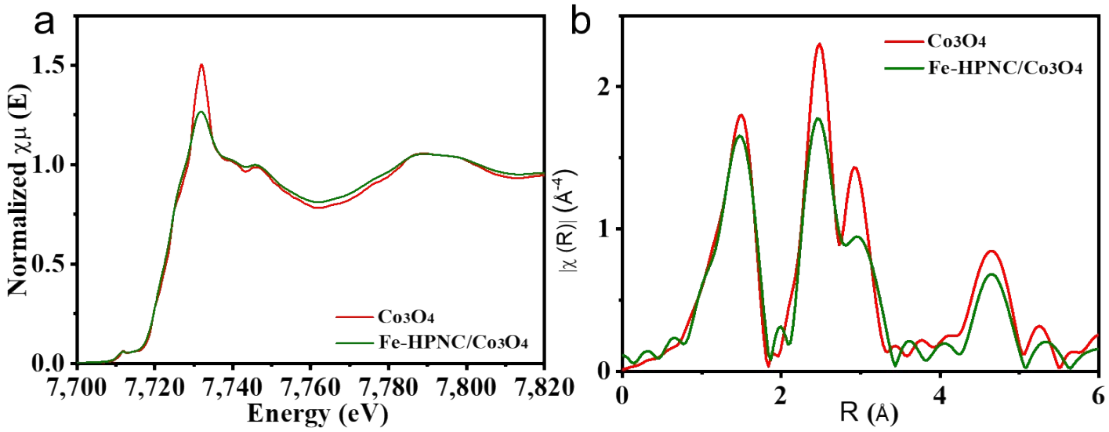

Fig. S16 Co k-edge **(a)** XANES spectra and **(b)** Fourier-transfer EXAFS spectra of Fe-HPNC/Co_3O_4 and commercial Co_3O_4.

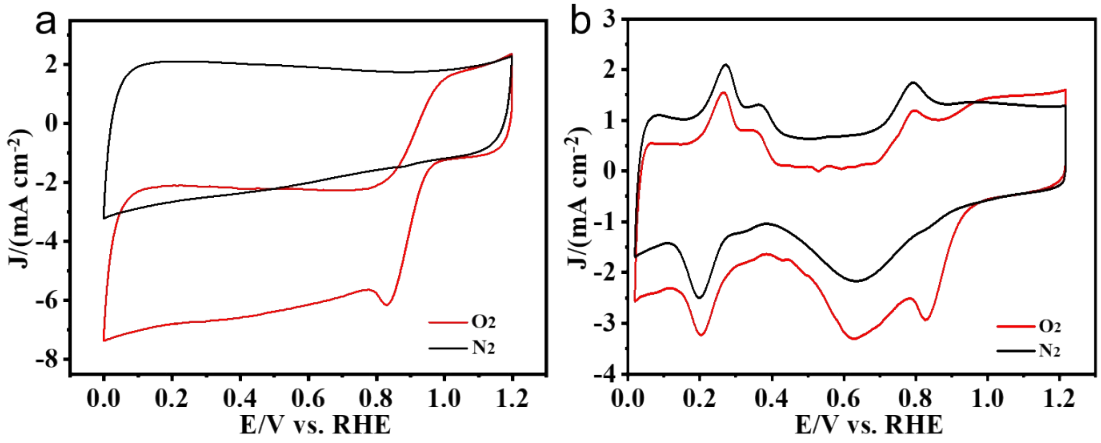

Fig. S17 Cycle voltammetry (CV) curves of **(a)** Fe-HPNC/Co_3O_4 and **(b)** Pt/C in 0.1 M KOH solution saturated with oxygen (red lines) and nitrogen (black lines). Scan rate: 50 mV s^{-1}.

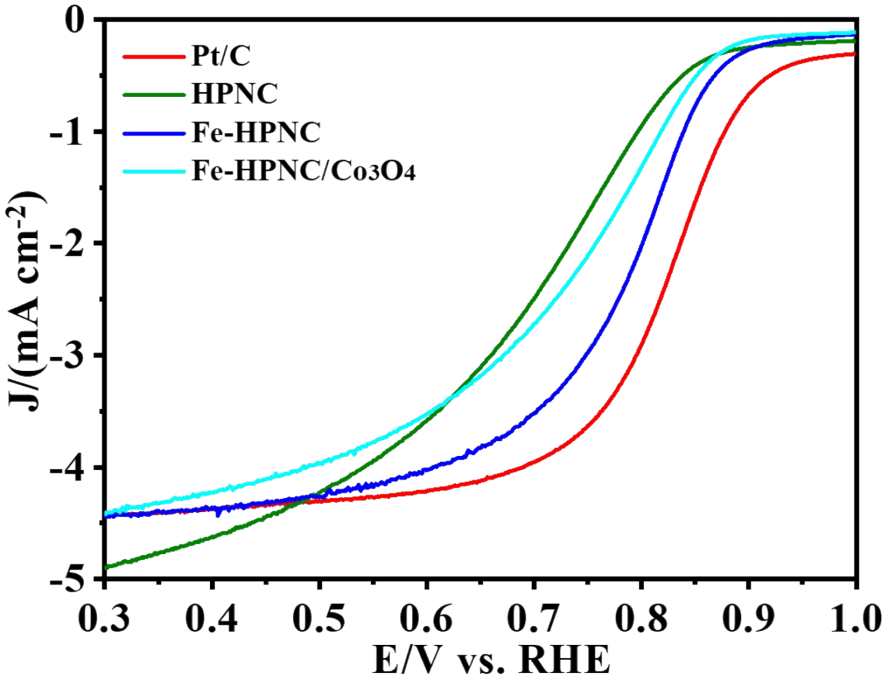

Fig. S18 ORR polarization curves of various catalysts in O_2-saturated 0.5 M H_2SO_4 solution with a rotating speed of 1600 rpm and a scan rate of 10 mV s^{-1}.

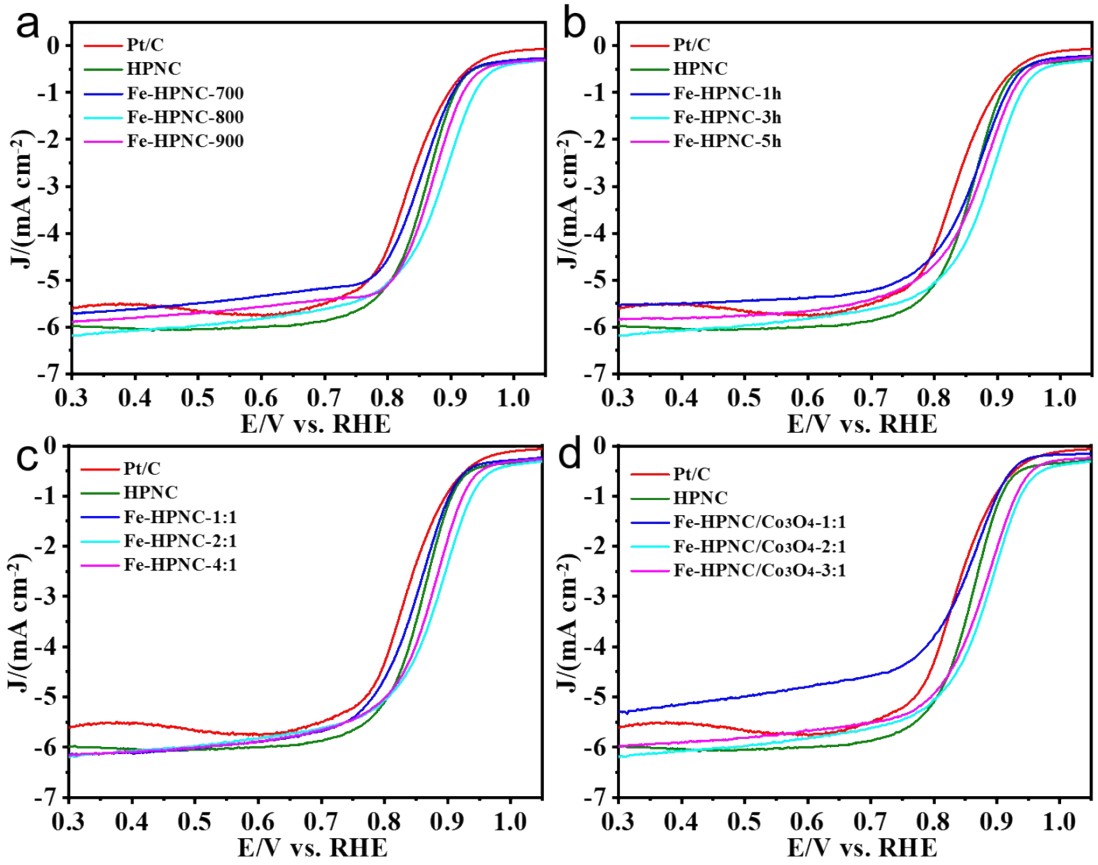

Fig. S19 ORR polarization curves of various catalysts synthesized with different **(a)** annealing temperature, **(b)** annealing time, **(c)** mass ratios of $FeCl_3$ to HPNC and **(d)** mass ratios of Fe-HPNC to Co_3O_4 in O_2-saturated 0.1 M KOH solution with a rotating speed of 1600 rpm and a scan rate of 10 mV s^{-1}.

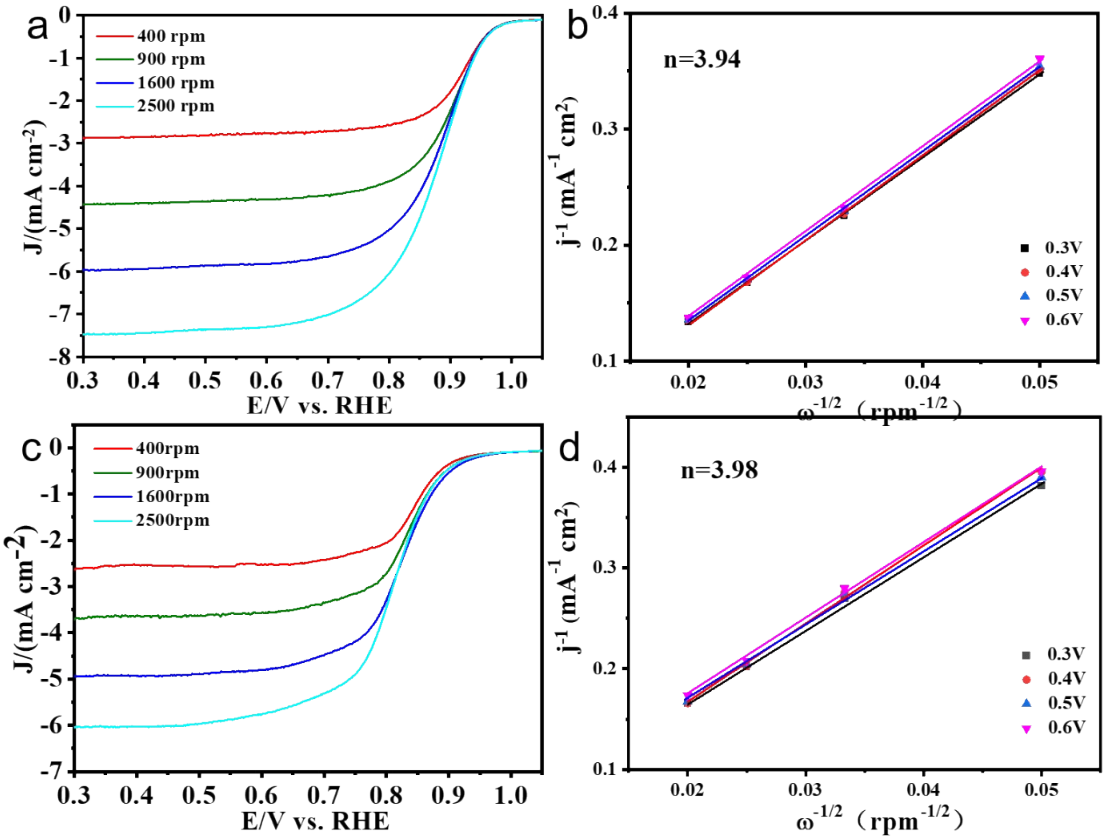

Fig. S20 ORR polarization curves at various rotating speeds and corresponding K-L plots at various potentials of **(a,b)** Fe-HPNC/Co3O4 and **(c,d)** Pt/C in O_2-saturated 0.1 M KOH solution.

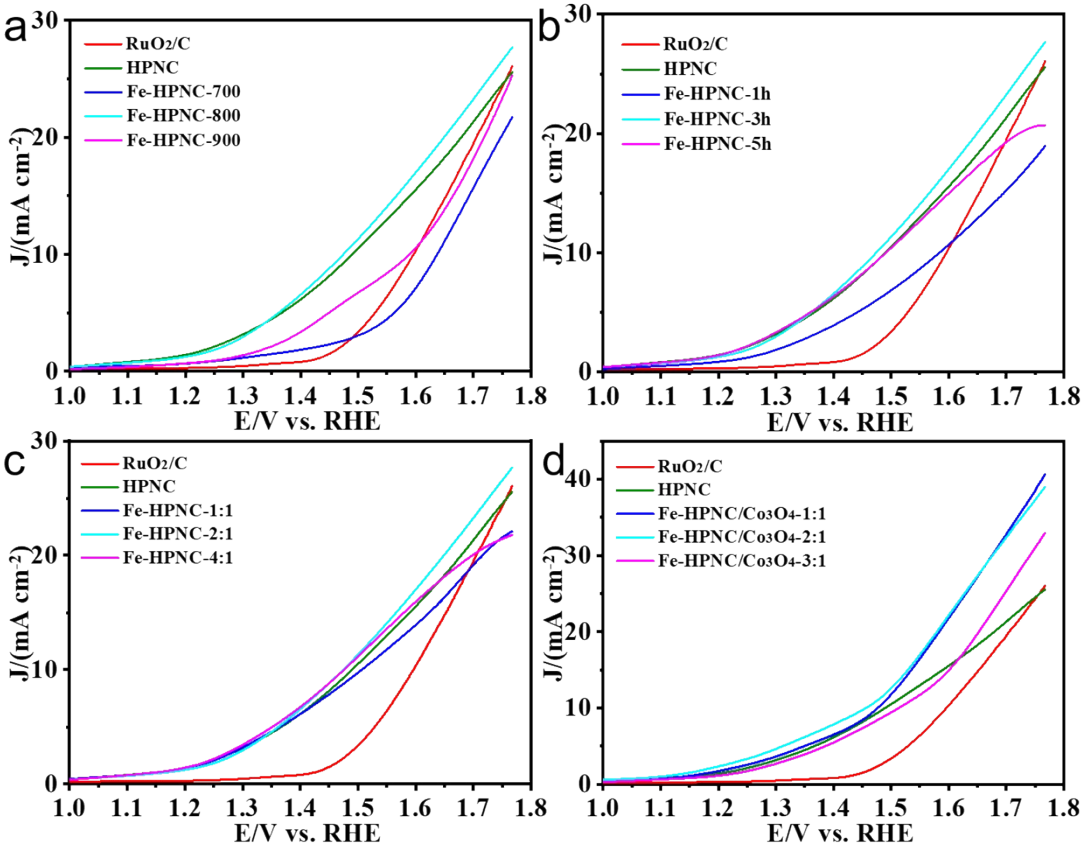

Fig. S21 OER polarization curves of various catalysts synthesized with different **(a)** annealing temperature, **(b)** annealing time, **(c)** mass ratios of $FeCl_3$ to HPNC and **(d)** mass ratios of Fe-HPNC to Co_3O_4 in O_2-saturated 0.1 M KOH solution with a rotating speed of 1600 rpm and a scan rate of 10 mV s^{-1}.

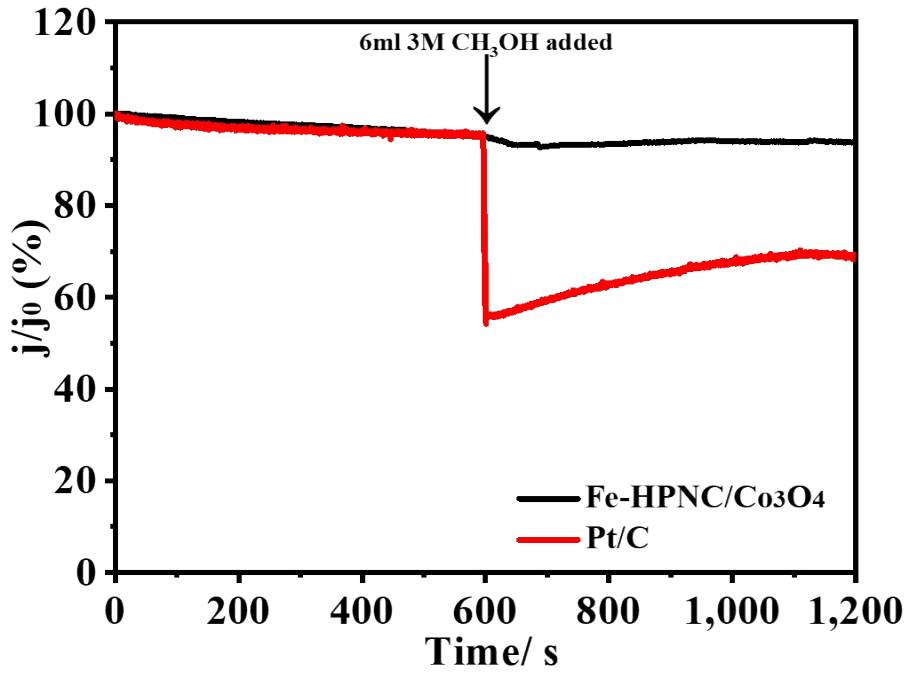

Fig. S22 ORR chronoamperometric responses of Fe-HPNC/Co_3O_4 and Pt/C at 0.65 V (vs. RHE) and 1600 rpm in O_2-saturated 0.1 M KOH solution with the addition of 6 ml 3 M methanol.

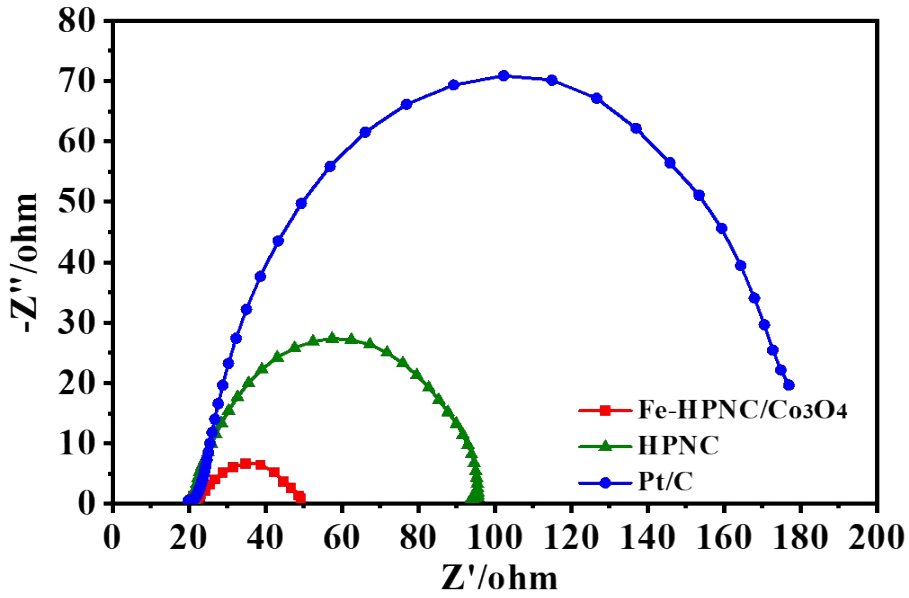

Fig. S23 Electrochemical impedance spectrum (EIS) of Fe-HPNC /Co_3O_4, HPNC and Pt/C at 0.85 V (vs. RHE) with the frequency ranging 10 kHz to 0.01 Hz and an amplitude of 5 mV in O_2-saturated 0.1 M KOH solution.

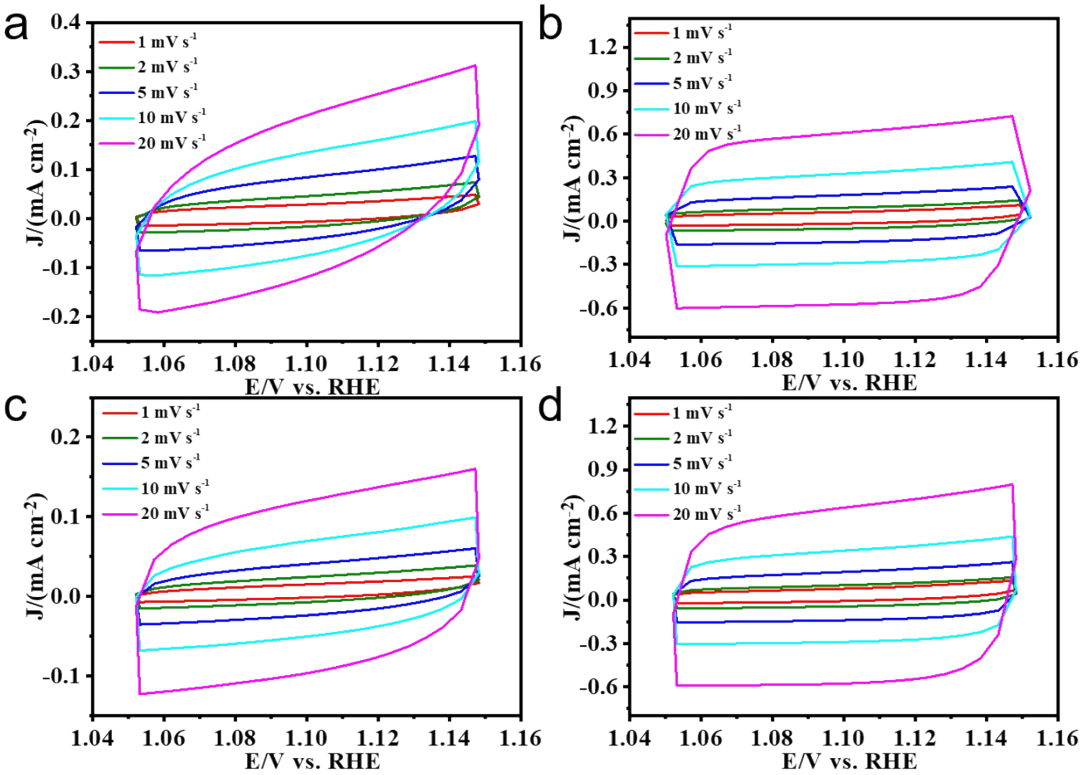

Fig. S24 CV curves of **(a)** Fe-HPNC-700, **(b)** Fe-HPNC-800, **(c)** Fe-HPNC-900 and **(d)** Fe-HPNC/Co_3O_4 with different scan rates in 0.1 M KOH solution.

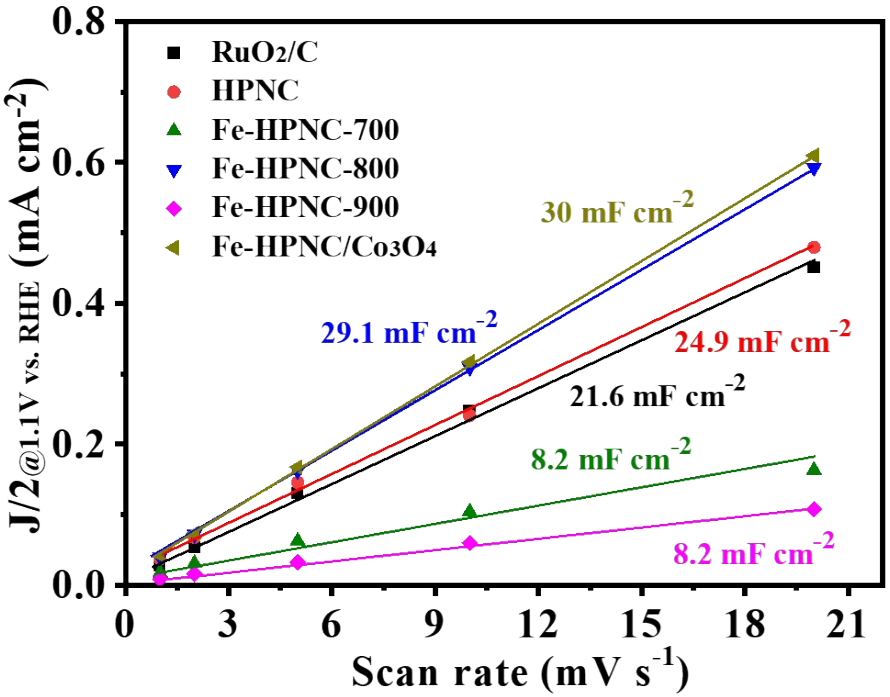

Fig. S25 Comparison of the electrochemical surface areas of various catalysts.

Fig. S26 Schematic illustration of the fabricated Zn-air battery.

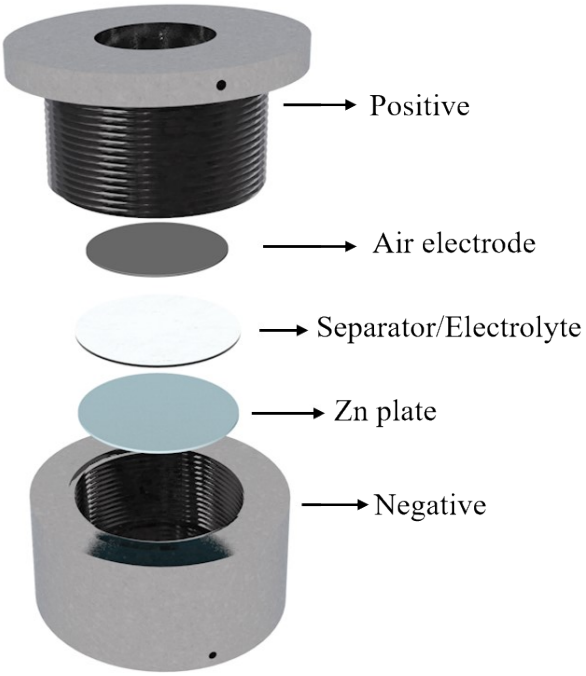

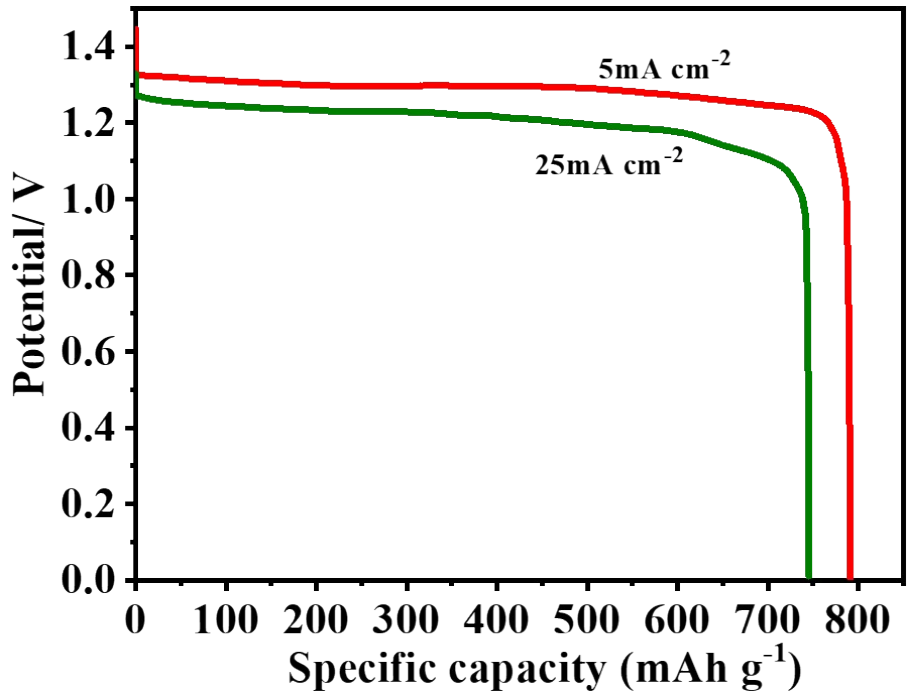

Fig. S27 Galvanostatic discharge curves of Zn-air battery employing Fe-HPNC/Co_3O_4 as cathodic catalysts at 5 mA cm^{-2} and 25 mA cm^{-2}.

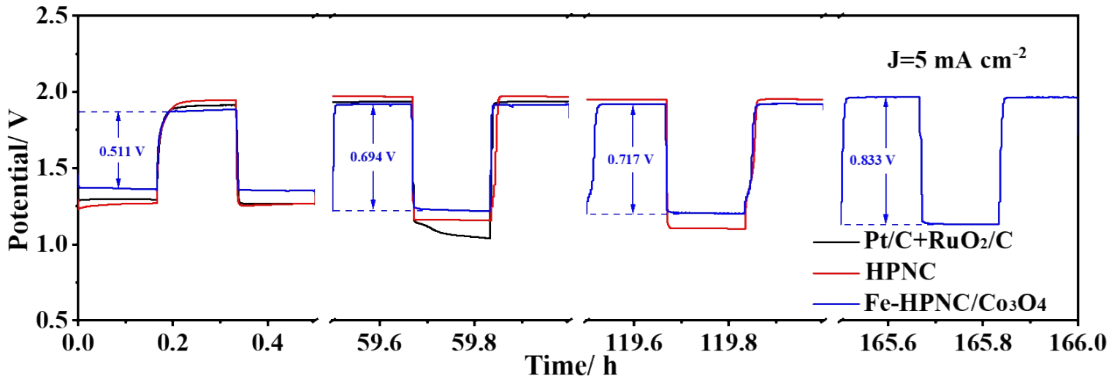

Fig. S28 Galvanostatic discharge-charge cycling curves of Zn-air batteries employing Pt/C+RuO_2/C, HPNC and Fe-HPNC/Co_3O_4 as cathodic catalysts at 5 mA cm^{-2} showing the changes of the voltage windows.

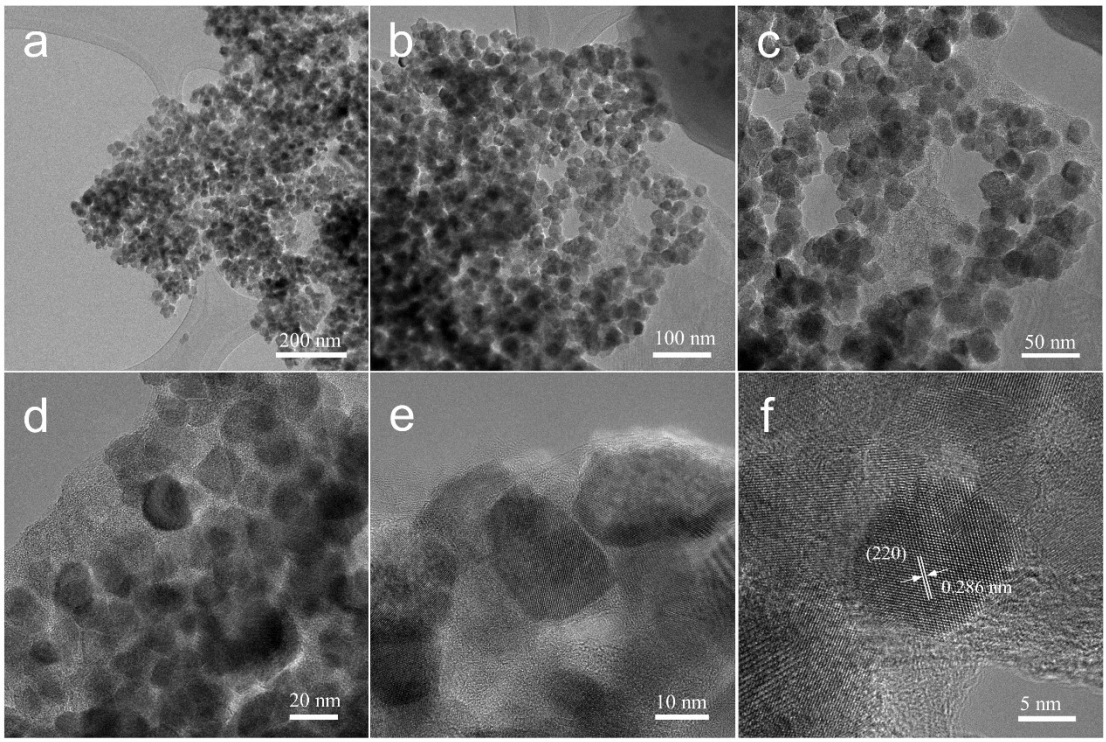

Fig. S29 (a-f) TEM and HR-TEM images of Fe-HPNC/Co_3O_4 after the long-term stability test of Zn-air batteries.

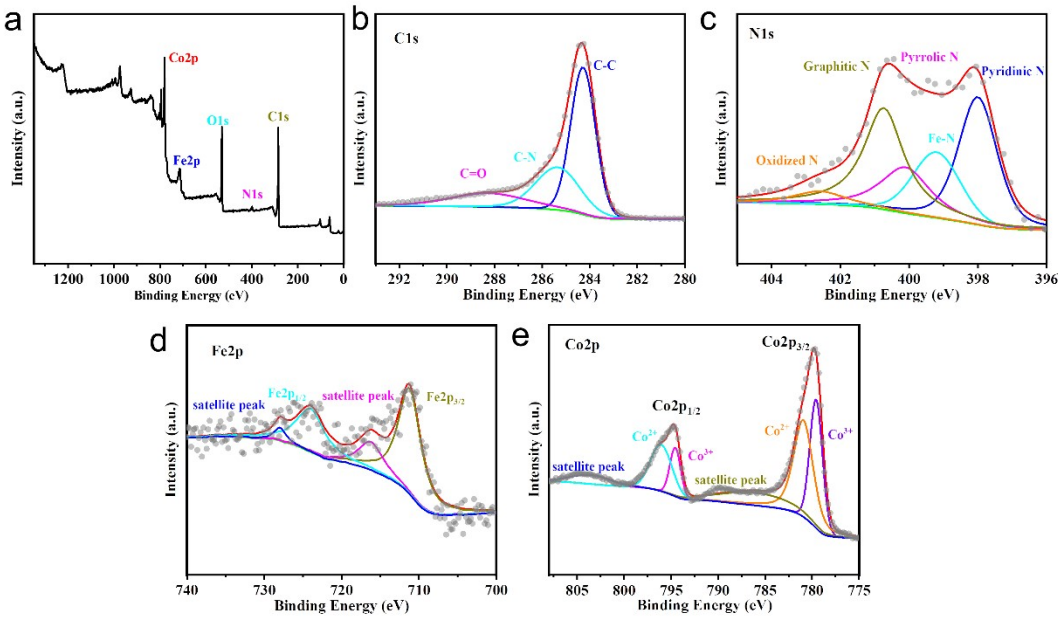

Fig. S30 (a) XPS survey spectra and high-resolution **(b)** C 1s, **(c)** N 1s, **(d)** Fe 2p and **(e)** Co 2p spectra of Fe-HPNC/Co_3O_4 after the long-term stability test of Zn-air batteries.

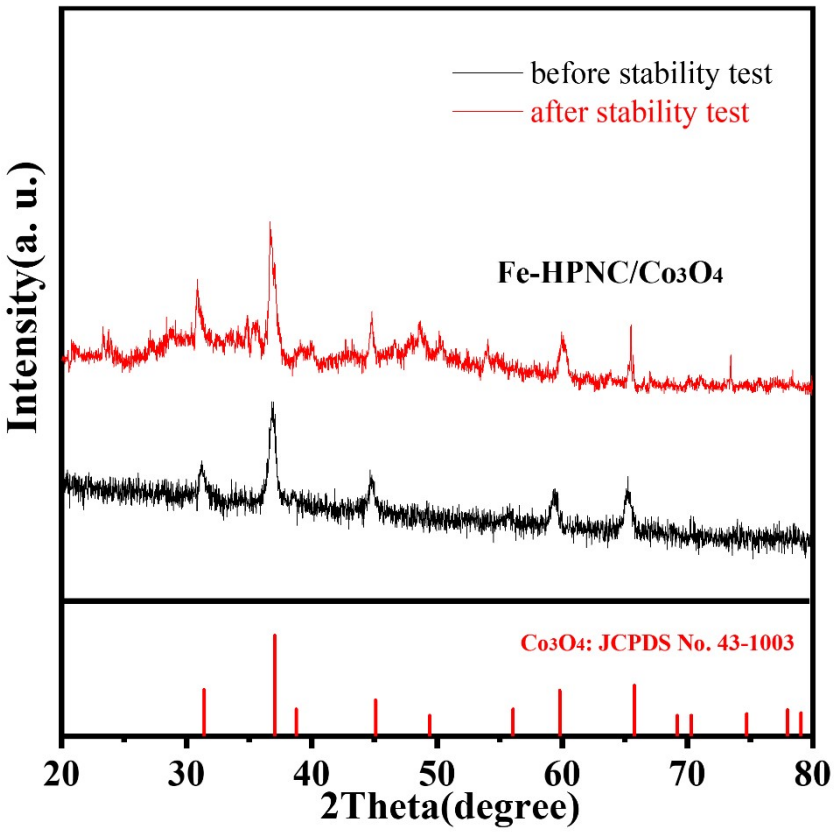

Fig. S31 XRD patterns of Fe-HPNC/Co_3O_4 before and after the long-term stability test of Zn-air batteries.

Table S1 Comparison of the porosity of various catalysts.

Sample	S_{BET} (m^2 g^{-1})	S_{micro} (m^2 g^{-1})	S_{meso} (m^2 g^{-1})	Total pore volume (cm^3 g^{-1})
Fe-HPNC	1083.831	224.441	859.39	2.661
Fe-HPNC/Co_3O_4	708.268	156.775	551.492	1.447
HPNC	1458.991	369.012	1089.98	2.617
Co_3O_4	61.493	49.511	11.912	0.197

Table S2 Elemental contents of various catalysts based on XPS results.

sample	C wt%	N wt%	O wt%	Fe wt%	Co wt%
Fe-HPNC-1:1	86.97	5.07	5.72	2.24	/
Fe-HPNC-2:1	86.23	4.67	5.67	3.45	/
Fe-HPNC-4:1	85.95	4.55	5.25	4.25	/
Fe-HPNC-700	83.73	4.8	6.56	4.31	/
Fe-HPNC-800	86.23	4.67	5.67	3.45	/
Fe-HPNC-900	87.79	4.54	5.48	2.19	/
Fe-HPNC/Co_3O_4	63.01	2.96	22.58	2.71	7.89

Table S3 Fe and Co contents of various catalysts based on ICP-OES results.

sample	Fe wt%	Co wt%
Fe-HPNC-1:1	0.34	/
Fe-HPNC-2:1	2.04	/
Fe-HPNC-4:1	2.84	/
Fe-HPNC-700	2.46	/
Fe-HPNC-800	2.04	/
Fe-HPNC-900	1.12	/
Fe-HPNC/Co_3O_4	1.56	7.29

Table S4 Fe K-edge EXAFS curve fitting parameters.

Samples	Path	C_N	R(Å)	σ^2(Å^2)	R factor
Fe-HPNC	Fe-N	1.6(6)	2.00	0.002(1)	0.02
	Fe-O	0.3(8)	2.16	0.005(2)	
	Fe-C1	1.2(6)	2.98	0.003(1)[a]	
	Fe-C2	0.8(4)	3.46	0.003(1)[a]	

C_N is coordination number; R is the distance between absorber and backscatter atoms; R factor indicates the goodness of the fit; σ^2 is Debye-waller factor. The Debye-waller factors were constrained as σ^2(Fe-C1) = σ^2(Fe-C2) for decreasing the correlation[a]. ΔE_0 is inner potential correction which is smaller than 10; S_0^2 is the amplitude reduction factor, which is fixed to be 0.75.

Table S5 Comparisons of Fe content, active sites and ORR performance for Fe-HPNC and other Fe-based single-atom catalysts.

Catalysts	Fe content (ICP-OES)	Active sites	$E_{1/2}$ (V vs. RHE)	Electrolyte	Ref.
Fe-HPNC	2.04 wt%)	FeN_2	0.886	0.1 M KOH	*This work*
Fe_{SA}-N-C	1.76 wt%	FeN_4	0.891	0.1 M KOH	1
Fe-Z8-C	3 wt%	FeN_4	0.871	0.1 M KOH	2
FeNCNs-800	0.44 at%	FeN_4 and	0.89	0.1 M KOH	3
SA-Fe-NHPC	1.25 wt%	FeN_x	0.93	0.1 M KOH	4
Fe SAC-MIL101-1000	1.27 wt%	FeN_x	0.94	0.1 M KOH	5
HSAC/Fe-3	2.78 wt%	FeN_4	0.814	0.5 M H_2SO_4	6
FeNC-CVD-750	2.0 wt%	FeN_4	0.85	0.5 M H_2SO_4	7
Fe, Mn/N-C	2.3 wt%	Fe, Mn-N_6	0.928	0.1 M KOH	8
KB-tpy-Fe-700	-	FeN_3	0.81	0.1 M KOH	9
Fe-N-C-900	0.66 at%	FeN_2	0.927	0.1 M KOH	10
Fe-SNC	0.34 at%	FeN_2	0.77	0.5 M H_2SO_4	11
FeCo/FeN_2/NH OPC	0.73 at%	Fe-N_2	0.86	0.1 M KOH	12
FeN_2-NOMC	0.5 at%	Fe-N_2	0.863	0.1 M KOH	13

Table S6 Comparisons of bifunctional electrocatalytic activities and the performance of the fabricated Zn-air batteries based on Fe-HPNC/Co_3O_4 and other recently reported non-noble metal catalysts.

Catalysts	$E_{1/2}$ (V vs. RHE)	$E_{j=10}$ (V vs. RHE)	ΔE (V)	Peak Power Density (mW cm^{-2})	Durability	Ref.
Fe-HPNC /Co_3O_4	0.886	1.457	0.571	236	165 h at 5 mA cm^{-2}	*This work*
HPNC	0.854	1.474	0.62	201	120 h at 5 mA cm^{-2}	14
Co_3O_4C-NA	0.78	1.52	0.74	-	-	15
Co@Co_3O_4/NC	0.80	1.65	0.85	-	-	16
Co_3O_4/NPGC	0.842	1.725	0.883	84	80 h at 5 mA cm^{-2}	17
Co_3O_4/CC	0.79	1.72	0.93	35	25 h at 3 mA cm^{-2}	18
Co_3O_4-NP/N-rGO	0.76	1.61	0.85	118	1000 min at 5 mA cm^{-2}	19
NC-Co_3O_4-90	0.87	1.588	0.718	82	210 h at 10 mA cm^{-2}	20
ZIF-L-D-Co_3O_4/CC	0.9	1.54	0.64	74	384 h at 5 mA cm^{-2}	21
CoO_x/N-RGO	0.896	1.6	0.704	120	10 h at 6 mA cm^{-2}	22
NP-Co_3O_4/CC	0.9	1.56	0.66	200	400 h at 5 mA cm^{-2}	23
Co/Co_3O_4@CoS-SNC	0.86	1.59	0.73	101	1000 min at 5 mA cm^{-2}	24
MnO/Co/PGC	0.78	1.6	0.82	172	75 h at 10 mA cm^{-2}	25
N-CoS_2-YSSs	0.81	1.6	0.79	81	165 h at 10 mA cm^{-2}	26
CNT@SAC-Co/NCP	0.87	1.61	0.74	172	210 h at 5 mA cm^{-2}	27

Table S7. Comparison of elemental contents of Fe-HPNC/Co_3O_4 before and after the cycling of Zn-air batteries according to XPS results.

sample	C wt%	N wt%	O wt%	Fe wt%	Co wt%
Fe-HPNC/Co_3O_4 (before cycling)	63.01	2.96	22.58	2.71	7.89
Fe-HPNC/Co_3O_4 (after cycling)	62.02	2.46	24.36	2.42	8.73

References

1 L. Jiao, G. Wan, R. Zhang, H. Zhou, S. H. Yu and H. L. Jiang, *Angew. Chem. Int. Ed.*. 2018, **57**, 8525-8529.

2 Q. T. Liu, X. F. Liu, L. R. Zheng and J. L. Shui, *Angew. Chem. Int. Ed.,* 2018, **57**, 1204-1208.

3 X. Ao, W. Zhang, Z. Li, L. Lv, Y. Ruan, H. Wu, W. Chiang, C. Wang, M. Liu and Zeng, X. *J. Mater. Chem. A,* 2019, **7**, 11792-11801.

4 G. Chen, P. Liu, Z. Liao, F. Sun, Y. He, H. Zhong, T. Zhang, E. Zschech, M. Chen, G. Wu, J. Zhang, X. Feng, *Adv. Mater.,* 2020, **32**, 1907399.

5 X. Xie, L. Peng, H. Yang, G. I. N. Waterhouse, L. Shang and T. Zhang, *Adv. Mater.*,2021, **33**, 2101038.

6 J. Guo, B. Li, Q. Zhang, Q. Liu, Z. Wang, Y. Zhao, J. Shui, Z. Xiang, *Adv. Sci.,* 2021, **8**, 2002249.

7 L. Jiao, J. Li, L. L. Richard, Q. Sun, T. Stracensky, E. Liu, M. T. Sougrati, Z. Zhao, F. Yang, S. Zhong, H. Xu, S. Mukerjee, Y. Huang, D. A. Cullen, J. H. Park, M. Ferrandon, D. J. Myers, F. Jaouen and Q. Jia, *Nat. Mater*., 2021, **20**, 1385-1391.

8 G. Yang, J. Zhu, P. Yuan, Y. Hu, G. Qu, B. Lu, A. Xue, X. H. Yin, W. Cheng, J. Cheng, W. Xu, J. Li, J. Hu, S. Mu and J. N. Zhang, *Nat. commun*., 2021, **12**, 1734.

9 M. F. Holly, I. I. Ebralidze, P. D. Meline, O. V. Zenkina and E. B. Easton, *J. Electrochem. Soc.,* 2020, **167**, 084520.

10 C. Zhu, Q. Shi, B. Z. Xu, S. Fu, G. Wan, C. Yang, S. Yao, J. Song, H. Zhou, D. Du, S. P. Beckman, D. Su and Y. Lin, *Adv. Energy Mater.,* 2018, **8**, 1801956.

11 H. Shen, E. G. Espino, J. Ma, K. Zang, J. Luo, L. Wang, S. Gao, X. Mamat, G. Hu, T. Wagberg and S. Guo, *Angew. Chem. Int. Ed.,* 2017, **56**, 13800-13804.

12 Y. Wang, M. F. Qiao and X. Mamat, *Chem. Eng. J.,* 2020, **402**, 126214.

13 H. Shen, E. G. Espino, J. Ma, H. Tang, X. Mamat, T. Wagberg, G. Hu and S. Guo, *Nano Energy,* 2017, **35**, 9-16.

14 F. Gui, Q. Jin, D. Xiao, X. Xu, Q. Tan, D. Yang, B. Li, P. Ming, C. Zhang, Z. Chen, S. Siahrostami and Q. Xiao, *Small,* 2022, **18**, 2105928.

15 T. Y. Ma, S. Dai, J. Mietek and S. Z. Qiao, *J. Am. Chem. Soc.,*2014, **136**, 13925-13931.

16 A. Aijaz, J. Masa, C. Rösler, W. Xia, P. Weide, A. J. R. Botz, R. A. Fischer and W. Schuhmann, *Angew. Chem. Int. Ed.,* 2016, **55**, 4087-4091.

17 G. Li, X. Wang, J. Fu, J. Li, M. G. Park, Y. Zhang, G. Lui and Z. Chen, *Angew. Chem. Int. Ed.,* 2016*,* **55**, 4977-4982.

18 Y. Li, C. Zhong, J. Liu, X. Zeng, S. Qu, X. Han, Y. Deng, W. Hu and J. Lu, *Adv. Mater.,* 2018, **30**, 1703657.

19 X. Han, G. He, Y. He, J. Zhang, X. Zheng, L. Li, C. Zhong, W. Hu, Y. Deng and T. Y. Ma, *Adv. Energy Mater.,* 2018, **8**, 1702222.

20 C. Guan, A. Sumboja, H. Wu, W. Ren, X. Liu, H. Zhang, Z. Liu, C. Cheng, S. J. Pennycook and J. Wang, *Adv. Mater.,* 2017, **29**, 1704117.

21 Y. Zhang, Z. Pan, X. Wang, J. Yang, Y. Qiu, S. Xu, Y. Lu, Q. Huang and W. Li, *Adv. Sci.,* 2019, **6**, 1802243.
22 T. Zhou, W. Xu, N. Zhang, Z. Du, C. Zhong, W. Yan, H. Ju, W. Chu, H. Jiang, C. Wu, Y. Xie, *Adv. Mater.,* 2019, **31**, 1807468.
23 X. Wang, Z. Liao, Y. Fu, C. Neumann, A. Turchanin, G. Nam, E. Zschech, J. Cho, J. Zhang, X. Feng, *Energy Stor. Mater.,* 2020, **26**, 157-164.
24 H. Pan, X. Huang, Z. Lu, Z. Zhang, B. An, D. Wu, T. Wang, X. Chen, F. Cheng, *Chem. Eng. J.,* 2021, **419**, 129619.
25 X. F. Lu, Y. Chen, S. Wang, S. Gao and X. W. Lou, *Adv. Mater.*, 2019, **31**, 1902339.
26 X. F. Lu, S. L. Zhang, E. Shangguan, P. Zhang, S. Gao and X. W. Lou, *Adv. Sci.*, 2020, **7**, 2001178.
27 J. C. Li, Y. Meng, L. Zhang, G. Li, Z. Shi, P. X. Hou, C. Liu, H. M. Chen and M. Shao, *Adv. Funct. Mater.*, 2021, **31**, 2103360.